

Thermomechanical behavior of Al-Cu-Si commercial alloy modified with rare earths

J. Camarillo-Cisneros^{a,*}, R. Pérez-Bustamante^b and R. Martínez-Sánchez^{c,*}

^aLaboratory of Computational Physical Chemistry, Facultad de Medicina y Ciencias Biomédicas, Universidad Autónoma de Chihuahua. Chihuahua, Chih., México.
e-mail: javier.camarillo@uach.mx

^bCONACYT-Corporación Mexicana de Investigación en Materiales S.A. de C.V., Eje 126 225, Industrial San Luis, 78395 San Luis, S.L.P., México.

^cCentro de Investigación en Materiales Avanzados, Laboratorio Nacional de Nanotecnología, Miguel de Cervantes No.120, C.P. 31109, Chihuahua, Chih., México.
e-mail: roberto.martinez@cimav.edu.mx

Received 27 March 2020; accepted 30 July 2020

Microstructural and mechanical effects were studied on automotive-grade 319 aluminum alloy after cerium/lanthanum rare earth additions at room and hot working conditions. Cerium/lanthanum additions formed micrometric phases in AA319, which were stable under room and hot working conditions. In comparison with reference alloy, Ce/La doped alloys reduced the eutectic-Si up to 85%. The effect of the Ce/La addition produced an increase in hardness and UTS under room temperature while improved mechanical performance in high-temperature working conditions. These improvements were attained to the presence of well-dispersed Ce/La micrometric needles, and the amount increase of θ' -phase (Al_2Cu) across the aluminum matrix. The θ' interfered directly with crack diffusion in the solid in two crystallographic directions. Additionally, it was observed through transmission electron microscopy, that Ce/La presence altered the precipitation kinetics in the formation of the coherent θ from the θ' .

Keywords: Cerium; lanthanum; aluminum.

DOI: <https://doi.org/10.31349/RevMexFis.66.782>

1. Introduction

The continuous development of suitable materials for use in large scale and continuous processes inside automotive, naval, and aerospace industries requires weight loss while still meeting mechanical standards. Among the modern metallic alloys, there are several aluminum alloys inside competitive prices and very well-known manufacturing processes. For manufacturing with mid-temperature thermal stability requirements (90-100°C) had been used commercial aluminum alloys belonging to $3xx.x$ series, precisely Al-Si-Cu chemical composition. Continuous improvement of mechanical properties inside $3xx.x$ alloys had been made by mapping thermal variables to found optimal solubilization [1], cooling rates, and aging conditions [2]. In this sense, the improvement of mechanical measures occurs due to microstructure modifications by thermal pathway; however, it also resorted to varying chemical composition. This last option can be listed doping of aluminum alloys by mono-element additions such: Ti, which caused the precipitation of the TiC phase with a positive impact in mechanical properties [3]. Additions of trace La in Al-Si alloys, which acts over Si, increasing elongation, and decreasing eutectic nucleation [4]. Partially inhibition has been reported in front of corrosion conditions acquired by the chemical environment or by high temperature thought additions of Ce due to CeO_2 formation [5]. In the case of multielement additions, we can enumerate TiB_2 that in the presence of dissolved Ti form TiAl_3 which acts as nucleation points for $\alpha\text{-Al}$ [6], causing a

remarkable mechanical improvement in Al-Si-Cu alloys [7]. However, there are reported a great variety of commercial aluminum alloys in combination with isolated or multielement additions that is not possible to extend predictions about the modified phase to extend to commercial aluminum alloys [8]. For example, the isolated use of La [9] or the use of Ce-mischmetal [10] in $3xx.x$ series improved creep resistance due to $\text{Al}_{11}\text{RE}_3$ precipitated across grain boundaries reducing dislocation motion producing positive effects Al-alloys. However, there is no consistency to ensure if $\text{Al}_{11}\text{La}_3$ was more stable than $\text{Al}_{11}\text{RE}_3$. This fact shows the need for study doping effect in every commercial alloy of interest.

In this work, we evaluated micro- and nanostructure modifications in aluminum alloy 319 (AA319) after the addition of Ce/La in low percent at room, high temperature, and after overhigh temperature conditions. The mechanical behavior was related to such microstructural changes employing stress and hardness tests.

2. Experimental procedure

The base materials consisted of AA319 ingot and Al-6Ce-3La master alloy. The conventional die casting process took place using 2 kg batches of AA319 melted at 720°C inside a graphite crucible carried out in an electric resistance furnace. After 30 minutes, the alloy was degassing by injecting Ar gas in conjunction with a graphite rotating impeller for 5 minutes. At the same process of degassing, nominal+5% of

Ce/La was added into the molten AA319 together with 0.33 wt.% Al-5Ti-B grain re-finer. Molten metal was poured into permanent metallic molds at 170°C and then cooled down to room temperature. Samples were heat-treated by solubilization during five hours at 495°C, followed by water quenching at 60°C and artificial aging at 220°C for three hours cooling down to room temperature in water (T6 condition). Thermally degraded samples were created heating at 250°C for 45 minutes and then evaluated at room temperature. For mechanical evaluation, it was carried out tensile tests on specimens with geometries according to the E8-ASTM standard on an Instron-337 universal testing machine at a constant displacement of 0.1 mm/s conducted at room and 250°C temperature. Hardness was measured in Wilson-Rockwell equipment using the Rockwell B scale limited to room temperature.

It was measured the chemical compositions by inductively coupled plasma atomic emission spectroscopy. Scanning electron microscopy (SEM, JEOL JSM-5800-LV) and high-resolution scanning transmission electron microscopy (HR-STEM, JEM-2200FS) were used to microstructural characterization. The processing of SEM specimens consisted of standard metallographic procedures and subsequently etched by 80/20 methanol/perchloric acid solution. HR-STEM specimens of 3 mm of diameter were electropolished employing TENUPOL twinjet equipment with 70% methanol -30% nitric acid at 20V and -30°C up to a thickness of 50 μ . X-ray diffraction patterns (XRD) were obtained in a Panalytical XPert-Pro Siemens D5000 model using CuK α radiation at 40 kV and 40 mA with a collection range from 15–90°C with a step of 0.026°. XRD patterns were Indexing by the Rietveld computational method. Volume crystal and microstress were calculated by Scherrer and Stokes-Wilson methods as implemented in FullProf code [11].

3. Results and discussion

Table I shows the chemical composition of all samples with the Cerium percentage defining each class. Cerium concentration remains at double of La content after the metallurgical process corresponding to 0.25, 0.5, and 1.0 at.%Ce with standard deviations of 1.2 to 2.0% from nominal values. Ce/La additions reduced iron content going from 0.7 at.% Fe in commercial AA319 to 0.58 at.%Fe in 0.25 at.%Ce, until higher addition of 0.50 at.%Ce and one at.% Ce shows just a

slight iron decrease to 0.55 at.%Fe on average. Regarding Cu and Si, both decreased linearly ($R^2 = 0.94$ and $R^2 = 0.99$, respectively) to Ce/La content; this is expected behavior due to affinity between Cu and rare earth.

Figure 1 shows SEM micrographs of as-cast (AC) and T6 thermal states through backscattering electron. The microstructure consists of Al-dendrites and eutectic silicon (ϵ -Si) as predominant phases as expected to standard casting process of $3xx.x$ alloys [12,13]. The aspect ratio and size of dendrites were similar in all compositions. Regarding microstructure of the ϵ -Si, it was notably refined after Ce/La addition since 0.25 to 1%Ce, contrasted in Fig. 1a (AA319_{AC}) and 1b) (0.5%Ce_{AC}) [14,15]. Due to the T6 thermal condition, ϵ -Si morphology continues the fragmentation process with smaller precipitates in Ce modified alloys, as shown in Figs. 1d) for 0.5%Ce_{T6}, Fig. 1e) shown quantification of ϵ -Si employing its average-area Si_{av} [16] in function of Ce/La additions at two thermal states. Decreasing of Si_{av} could affect kinetic of microfracture diffusion, a desired characteristic to extend the resistance to failure in Al alloys. As shown by a blue line in Fig. 1e), the behavior of Si_{av} in as-cast was modified from AA319_{AC} to 0.25%Ce_{AC} going from 30 μm^2 to 14 μm^2 , posterior reduction in 0.5%Ce_{AC} resulting in Si_{av} of 11 μm^2 and kept until 1%Ce_{AC}. In the case of the T6 condition (red line), a slight decrease in Si_{av} was obtained in comparison to its previous thermal stage just for Ce/La modified alloys together to aspect ratio change. In the case of A319_{T6} in Fig. 1c shown aspect ratio modification at the time that Si_{av} was maintaining. The precipitation of the ϵ -Si particles is due to Ostwald ripening or coarsening [17], a process that states that the observed ϵ -Si particles would be the result of a two-stage process. I) Si atoms in the supersaturated solution, create bonds and solidify as the temperature decreases. II) The solidified particles appear on nucleation points, in the case of AA319 on TiB₂. The subsequent growth of ϵ -Si took place from the binding of precipitates of the same chemical composition. The nucleation rate of ϵ -Si depends on temperature and time so that it produces a widespread regarding precipitates distribution throughout the aluminum matrix. Due to the thermal treatment that follows solidification, the ϵ -Si precipitates can diffuse into the aluminum matrix. As a thermodynamic consequence of decreasing the surface energy, they increase in size. The Ce/La additions are highly thermal stable and influenced stage II of coarsening, providing more

TABLE I. Chemical compositions of AA319 and modified alloys in atomic percent. Left labels refer to Ce content until La contents were maintained between 0.53 to 0.54 fraction of Ce.

	Ce	La	Si	Cu	Fe	Zn	Mg	Mn	Zn	Ni	Al
Base AA319	–	–	7.94	2.51	0.70	0.39	0.33	0.25	0.39	0.04	
+0.25%Ce	0.255	0.136	7.70	2.28	0.58	0.39	0.36	0.28	0.39	0.02	bal
+0.5%Ce	0.506	0.272	7.45	2.09	0.57	0.36	0.33	0.25	0.36	0.02	
+1%Ce	1.012	0.556	6.75	1.93	0.51	0.35	0.30	0.23	0.36	0.02	

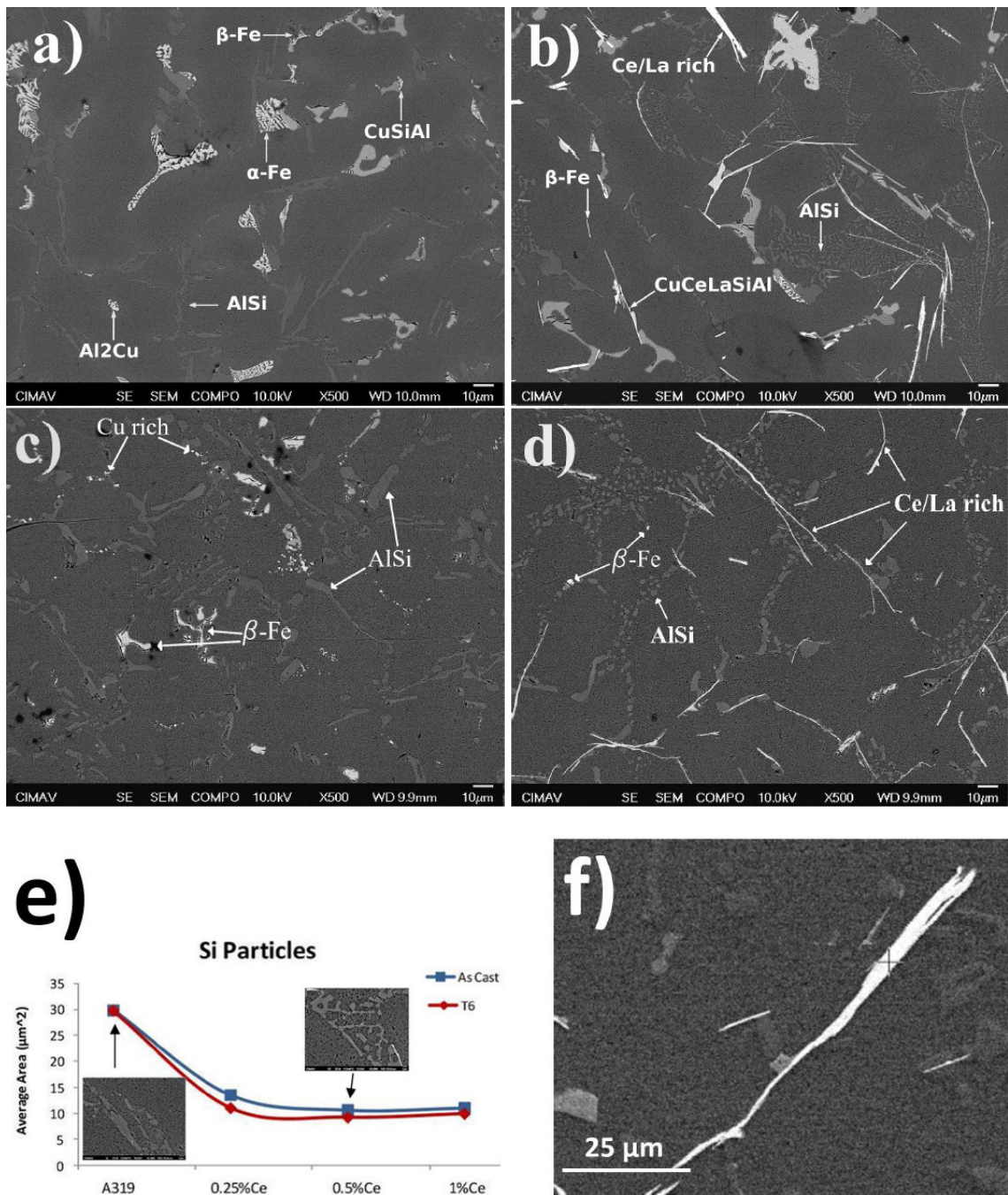


FIGURE 1. Micrographs obtained by Scanning Electron Microscopy in backscattered electron mode: a) as cast AA319, b) as cast AA319+0.5% Ce, c) T6-AA319, d) T6-AA319+0.5% Ce; Rare earth needles and β -Fe not suffer significant changes due to the employed thermal scheme with a maximum temperature of 495°C. e) Eutectic Si phases average-area, measures were reduced function of the Ce/La percent, f) Ce/La-rich needle over aged after 100 h at 250°C.

nucleation centers from which ε -Si growth. Ce/La influences the heat treatment by interfering with the free Si diffusion pathway and consequently decreasing the growth kinetics of ε -Si. In all, our alloys were observed harmful Fe-rich intermetallic as an inherent consequence of it is a component in chemical composition [18]. Iron precipitated in two phases distinguishable by morphology and size: AlFeSiCu in Chinese-script morphology (α -Fe) and AlFeSiCu with

needle-like morphology (β -Fe) [19]. Mn [20] and Mg [21] elements caused the initial reductions of β -Fe and reduced their decrepit effect [22]. In a synergistic effect by Ce/La additions, it was causing Fe fractionating into small noodles as a second reduction stage. The addition of cerium to AA319 caused the formation of Fe-intermetallics and the refinement of the microstructure. Modification of β -Fe particles must occur during the casting stage, concluded by the fact that

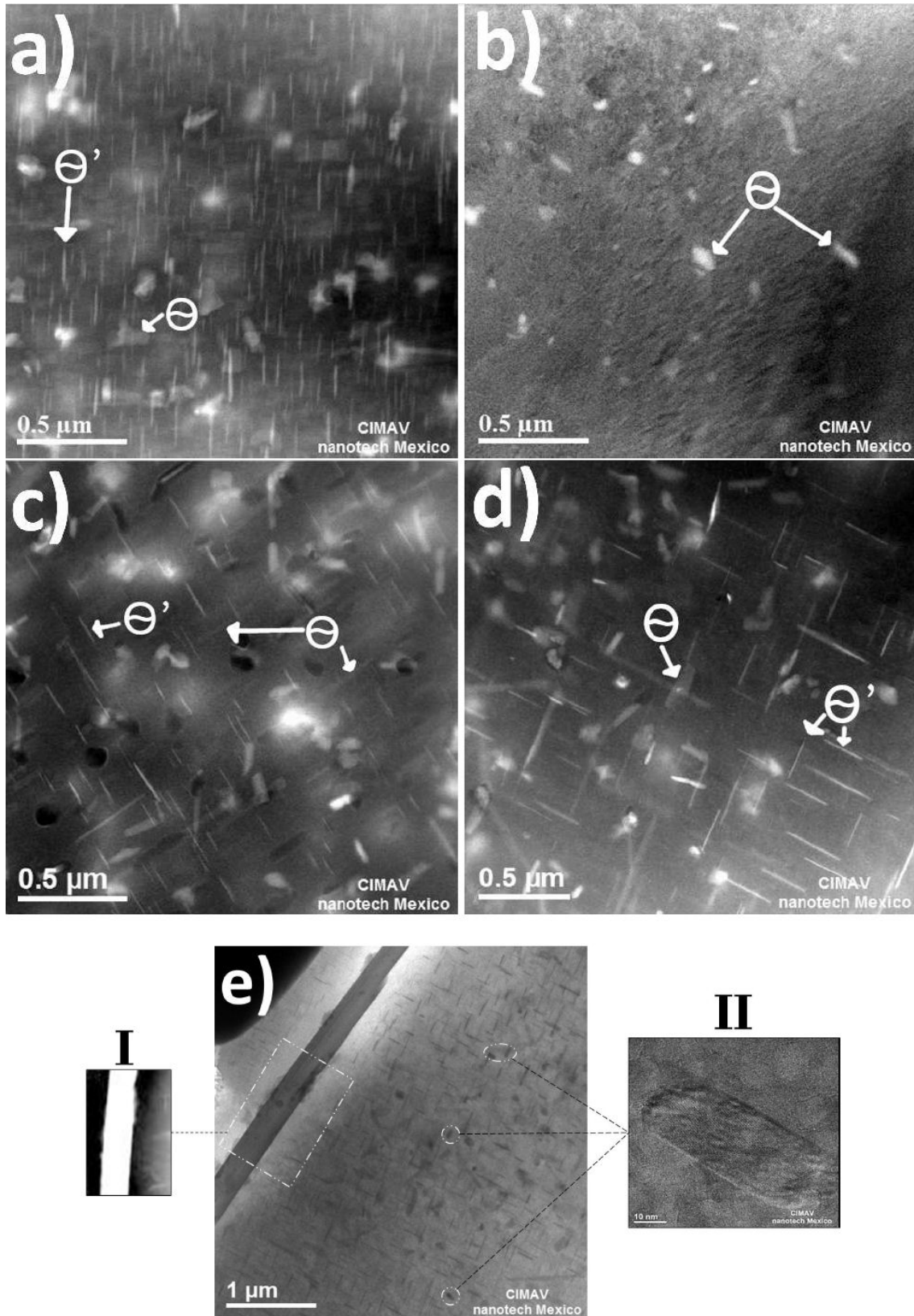


FIGURE 2. High resolution-STEM micrographs of compositions; a) AA319_{T6}, b) AA319_{OA}, c) 0.5%Ce_{T6} and d) 0.5%Ce_{OA}. At T6 state, Cu blocks like phase are presented in greater amounts in the unmodified sample while Ce/La addition creates a greater amount of θ' needles phase. In WT (250°C until 30 minutes), modified Ce/La samples preserved a greater amount of phase q and θ'.

Fe-intermetallics were thermally stable during the entire heat treatment. Fragmentation of β -Fe particles could decrease its harmful affect regarding mechanical properties. Ce/La additions were not producing noticeable surface differences regarding pore defects [23-25] or grain refinement [26] following other publications. Regarding modified alloys were observed precipitates of Ce/La in needles-like morphology to both as-cast (Fig. 1b) and T6 (Fig. 1d) stages. At both thermal states, Ce/La needles maintained a constant aspect ratio and a size ranging from 20-50 μm long and 15 μm wide-spreading along with the Al matrix. From Ce/La needles (Fig. 1f) elemental composition, the atomic percent averages of ten measurements were 10.21Si, 0.95Fe, 0.91Ni, 23.85Cu, 4.4La, 7.51Ce (Al-bal). Ce/La needles were highly thermal stable being not affected by their initial morphology or aspect ratio by the heat treatment, not even by the long aging time up to 100 hours.

Figures 2a) and 2c) showed by HR-STEM microstructures in T6 condition to commercial AA319_{T6} and 0.5%Ce_{T6}, respectively. Micrographs contain needle-shaped particles with the chemical composition of Al₂Cu. In both, Fig. 2a) and Fig. 2c), θ' precipitates were within typical dimensions corresponding to the T6 treatment [27], and morphologies quite similar in range inside 50–200 nm AA319_{T6} in Fig. 2a) presents a higher density of θ' needles; nevertheless, 0.5%Ce_{T6} in Fig. 2c) contains the highest amount of θ' pairs. Strengthening of AA319 alloys is due to precipitation of Al₂Cu after T6 heat treatment in θ' with [0 0 1] orientation regarding the Al matrix [28]. θ' enhancement is a consequence of hinders dislocation movements inside the Al matrix at the nanoscale. To observe alloy degradation due to high-temperature T6 samples were held until 45 minutes at 250°C to create over-aged (OA) conditions. Figure 2b) shows OA effect on AA319_{OA} with microstructural changes concerning of high percentage of θ' transformed to θ . Also, Fig. 2b) shows the particle size coarsening of θ , similar to published references for high-temperature analog alloys [29,30]. Regarding the OA effect in 0.5%Ce_{OA} in Fig. 2d). It was observed a higher quantity of θ' than reference AA319 in Fig. 2b) at the same OA. There was a noticeable increase in the number of θ' needles and remaining in two equivalent crystallographic directions with very close morphology to its previous thermal state 0.5%Ce_{T6} of Fig. 2c). Even though θ' is uniformly distributed in-side Al matrix in modified 0.5%Ce_{OA} alloy, there was a marked discontinuity in Ce/La needle's vicinities, as shown in Fig. 2e). Using Z-contrast mode was verified the absence of θ' needles by a closer analysis, as shown in Fig. 2e)-I where dark zones correspond to the Al matrix while Ce/La and Cu precipitates correspond to white areas. The interface between Ce/La needle and the aluminum matrix is empty of θ' particles over a distance of 2 microns. However, due to the high atomic percent of copper in the Ce/La needles, it could be concluded that Cu around Ce/La needles diffuses to inside the needles in accordance to chemical composition of whit 23.85 at.% Cu. Even the long averaging of 100 hours at 250°C does not modify

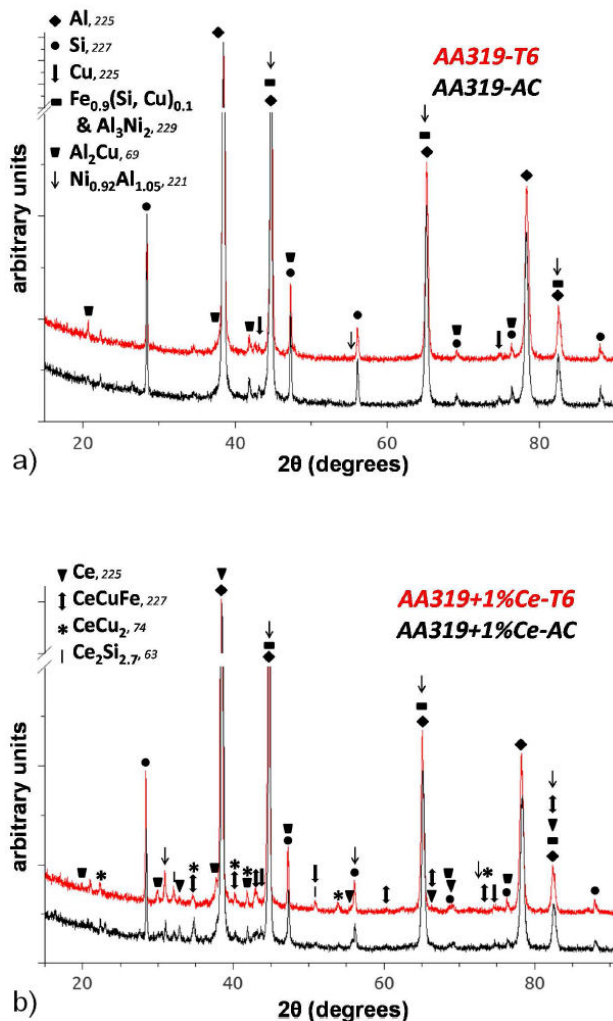


FIGURE 3. X-ray diffraction pattern, the upper panel corresponds to reference AA319; the lower panel contains the composition 1%Ce. The as-cast state (black lines) and T6 heat treatment (red lines) mainly show changes in diffracted intensities. The subscript beside each prototypical phase corresponds to the space group.

the Cu percent in Ce/La needles; thus, the mentioned Cu diffusion must occur in the stages of synthesizing and close to Ce/La needle. Figure 2e)-II shows Al-Cu precipitates thickened at T6 condition for 0.5%Ce_{OA} alloys with preferential orientation as θ' consistent with Al₂Cu closer to the description of Ω by its similar morphology to θ' .

Figure 3 concentrates the phase indexing from XRD and Rietveld method: AA319 reference (3a) and the maximum 1.0%Ce addition (3b) in AC and T6 stages. Employing the Inorganic Crystal Structure database, these were identified: Al(240129), Si(94261), Cu(53247), Fe_{0.9}(Si, Cu) (103624 and 102893), 4Al₂Cu(107544), Al₃Ni₂(608795) and Al_{1.05}Ni_{0.92}(608795) phases. As shown in Fig. 3a), the Al and Si crystals are the elements found with the highest percentage, as was expected. From the alloys in the AC to T6 stages, the heat treatment modified peaks ratio with no significant additional diffraction peaks. For 1%Ce_{T6} sample (Fig. 3b)) at the AC stage diffraction peaks cor-

responding to Ce/La elements identified were; Ce(41823), CeCuFe(102130), CeCu(62083) and CeSi(73065). Similar to the AA319 reference alloy, the main difference between AC and T6 was the peak ratio. There were no measurable changes in Al crystals with a volume in average dimensions crystal of 580\AA^3 using the solidification rate as a fixed parameter [31,32]. On the other hand, micro-stress slightly increases proportionally to the Ce/La amount from 25% to a maximal of 36% when adding 1.0% ACL, which variation comes from the incoherent interaction between Al matrix and Ce/La needles.

Microstructural changes due to Ce/La addition create notorious mechanical modifications screened through hardness and UTS tests. Hardness results from Fig. 4a) show an apparent enhancement dependent of Ce/La percentage at the as-cast condition. This modification was related to the hard Ce/La micro-needles precipitates, which spread uniformly in Al-matrix, so the higher the amount of cerium/lanthanum, the greater the number of micro-precipitates and the hardness value. Aging samples at the T6 stage displayed an average value of 54 Rockwell B with a drastic hardness increase in AA319_{AC} from 38 RB to 53 RB AA319_{T6} due to the precipitation of θ' phase. The addition of Ce/La in 0.25%Ce_{T6} resulted in lower hardness than reference, and only additions of 0.5%Ce_{T6} and 1%Ce_{T6} were improved. The additional strengthening observed in 0.5%Ce_{T6} and 1%Ce_{T6} were due to simultaneous contribution provided by Ce/La-rich and θ' phases. Thermal degradation in over-aged condition produces a decrease in the hardness behavior of all specimens, and with little effect on Ce/La samples from which 0.25%Ce_{T6} presented the maximum hardness, however, it is inside the resulting error of 0.5%Ce_{T6} and 1%Ce_{T6}.

The UTS results concentrated in Fig. 4b show for AC status the AA319 with the best performance of the four alloys due to the sharp morphology of Ce/La needles acts as crack propagators and is responsible for the mechanical failure [33]. On the other hand, after the T6 heat treatment, the AA319 – 1 %Ce modified samples present the maximum UTS value. Under this thermal state, the higher proportion of θ' pairs is interfering in two crystallographic directions, contrary to sample AA319, which possess one preferential orientation, as shown in Figs. 2a and 2c. UTS results in T6 for the modified samples was driven by the change in precipitation kinetics after the additions of rare earth, allowing a definite improvement just to 1%Ce_{T6}.

A decrease in Cu contents showed in Table I could suppose a negative effect on mechanical behavior by limitation of available atoms involved in hardening mechanisms; however, it was an improvement in mechanical properties presented in the result section. At over aging condition was observed a reduction in mechanical falling rate in 0.25%Ce_{OA} and 0.5%Ce_{OA} additions in comparison to AA319_{OA}. Crystal stability at this condition is in agreement with T6 heat treatment, due to the high quantity of θ' remaining after the high thermal state. Even for the case of isolated Ce addition

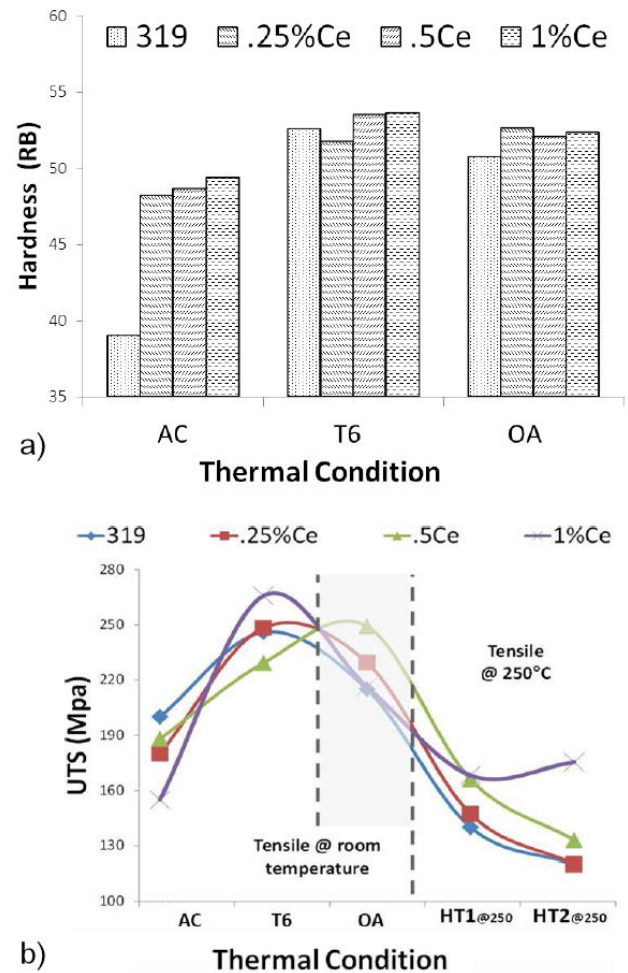


FIGURE 4. Hardness measures in the Rockwell B scale corresponding to the four employed chemical compositions at thermal states; as-cast, solubilized + aged (T6), and OA measured at room conditions. b) Ultimate tensile strength for 319 aluminum alloy and 0.25%, 0.5%, and 1%Ce. Tests performed at room temperature were; as-cast, T6, and working temperature while HT1@250°C and HT2@250°C refers to samples after maintaining the alloys until 45 min at 250°C.

has been observed modified precipitation kinetic of α -Al to lower temperatures and improvement in tensile strength and hardness [34]. As a complementary test, additional tensile tests carried out under hot working conditions HT1 and HT2. For HT1 the tensile test was carried out at 250°C, showing UTS results proportional to the amount of Ce/La additions: $1\%Ce_{HT1} > 0.5\%Ce_{HT1} > 0.25\%Ce_{HT1} > AA319_{HT1}$. A second experiment at 250°C, called HT2, was performed at greater solubilization temperature of 520 °C. The results were an increase in the amount of dissolved Cu but a decrease in the number of θ' needles. The obtained trend of UTS was close similar than HT1: $1\%Ce_{HT2} > 0.5\%Ce_{HT2} > 0.25\%Ce_{HT2} \approx AA319_{HT2}$. Since were realized the stress tests at temperatures close to Cu melting point, the alloys were mostly affected as it contains less θ' precipitated. The only alloy improved was 1%Ce_{HT2} due to the kinetics reduced by the presence of Ce/La.

4. Conclusions

The effects of cerium and lanthanum additions in the automotive-grade commercial aluminum alloy 319 were microstructurally and mechanically studied. The ϵ -Si average area was noticeably reduced in size in the initial as-cast condition, with a small additional reduction after subsequent thermal treatment. A more rounded morphology in ϵ -Si and Si_{av} was in function of the Ce/La addition. Ce and La precipitated in needle-like phases at the micrometric scale, being responsible for the hardness enhancement at all thermal states. There was a higher quantity of θ' needles pairs at the nanoscale in Ce/La samples. Under working conditions (T6 and OA), rare earth additions improved both hardness and UTS; this is due to that Ce/La alters the kinetic of precipitation rate from θ' to the stable θ . The addition of Ce/La af-

fects the hardening process and shows improvements in high-temperature tensile tests. Instead, θ' thickened in AA319 was the main reason for strengthening lost. Doped AA319 presented mechanical improvement as a function of thermal history until reaching T6 heat treatments. Cerium-lanthanum doping elements had the effect of reducing mechanical degradation after material exposition at 250°C. Optimal Ce/La in UTS tests were 1%Ce in T6, 0.5Ce in over-aged, and 1%Ce until high temperature. Thus Ce/La doping, in conjunction with the T6 thermal treatment scheme, is applicable for high-temperature applications.

Acknowledgments

The authors are grateful to CONACYT for 290674 and 290604 scholarships.

1. E. Cerri, E. Evangelista, S. Spigarelli, P. Cavaliere, and F. Dericcardis, Effects of thermal treatments on microstructure and mechanical properties in a thixocast 319 aluminum alloy, *Mater. Sci. Eng. A* **284** (2000) 254. [https://doi.org/10.1016/S0921-5093\(00\)00748-6](https://doi.org/10.1016/S0921-5093(00)00748-6).
2. F. Tavitans-Medrano, J. Gruzleski, F. Samuel, S. Valtierra, H. Doty, Effect of mg and sr-modification on the mechanical properties of 319-type aluminum cast alloys subjected to artificial aging, *Mater. Sci. Eng. A* **480** (2008) 356. <https://doi.org/10.1016/j.msea.2007.09.002>.
3. A. Contreras and E. Bedolla, Fabricacion y caracterizacion de materiales compuestos de matriz metalica al-cu y al- mg reforzados con particulas de tic, *Rev. Mex. Fis.* **50** (2004) 495.
4. Y.-C. Tsai, C.-Y. Chou, S.-L. Lee, C.-K. Lin, J.-C. Lin, S. Lim, Effect of trace la addition on the microstructures and mechanical properties of aa356 (al-7si-0.35mg) aluminum alloys, *J. Alloys Compd.* **487** (2009) 157. <https://doi.org/10.1016/j.jallcom.2009.07.183>.
5. P. M. Ashraf, and S. M. A. Shibli, Reinforcing aluminium with cerium oxide: A new and effective technique to prevent corrosion in marine environments, *Electrochem. Commun.* **9** (2007) 443. <https://doi.org/10.1016/j.elecom.2006.09.010>.
6. P. S. Mohanty, and J. E. Gruzleski, Mechanism of grain refinement in aluminium, *Acta Metall. Mater.* **43** (1995) 2001. [https://doi.org/10.1016/0956-7151\(94\)00405-7](https://doi.org/10.1016/0956-7151(94)00405-7).
7. Kh. A. Ragab *et al.*, Influence of fluidized sand bed heat treatment on the performance of Al-Si cast alloys, *Mater. Des.* **32** (2011) 1177. <https://doi.org/10.1016/j.matdes.2010.10.023>.
8. M. Easton, and D. StJohn, Grain refinement of aluminum alloys: Part i. the nucleant and solute paradigms a review of the literature, *Metall. Mater. Trans. A* **30** (1999) 1613. <https://doi.org/10.1007/s11661-999-0098-5>.
9. I. A. Anyanwu *et al.*, Effect of substituting cerium-rich mischmetal with lanthanum on high temperature properties of die-cast Mg-Zn-Al-Ca-RE alloys, *Mater. Sci. Eng. A* **380** (2004) 93. <https://doi.org/10.1016/j.msea.2004.03.039>.
10. J. Zhang *et al.*, Effect of substituting cerium-rich mischmetal with lanthanum on microstructure and mechanical properties of die-cast Mg-Al-Re alloys, *Mater. Des.* **30** (2009) 2372. <https://doi.org/10.1016/j.matdes.2008.10.028>.
11. J. Rodríguez-Carvajal, Recent advances in magnetic structure determination by neutron powder diffraction, *Physica B* **192** (1993) 55. [https://doi.org/10.1016/0921-4526\(93\)90108-1](https://doi.org/10.1016/0921-4526(93)90108-1).
12. H. Kaya, E. Çadirli, M. Gündüz, Dendritic growth in an aluminum-silicon alloy, *J. Mater. Engin. Perform.* **16** (2007) 12. <https://doi.org/10.1007/s11665-006-9002-2>.
13. W. Donlon, Precipitation of aluminum in the silicon phase contained in W319 and 356 aluminum alloys, *Metall. Mater. Trans. A* **34** (2003) 523. <https://doi.org/10.1007/s11661-003-0088-y>.
14. G. García-García, J. Espinoza-Cuadra, H. Mancha-Molinar, Copper content and cooling rate effects over second phase particles behavior in industrial aluminum-silicon alloy 319, *Mater. Des.* **28** (2007) 428. <https://doi.org/10.1016/j.matdes.2005.09.021>.
15. M. Lalpoor, D. Eskin, G. ten Brink, and L. Katgerman, Microstructural features of intergranular brittle fracture and cold cracking in high strength aluminum alloys, *Mater. Sci. Eng. A* **527** (2010) 1828. <https://doi.org/10.1016/j.msea.2009.11.003>.
16. The measurements corresponds to Si particles mean surface (S1) obtained from an approximate area of 11000 square micrometers (200 × 10 images per sample).
17. W. Ostwald, The theory of ostwald ripening, *Z. Phys. Chem.* **37** (1901) 385.

18. D. Mitlin, J. Morris, J.W., V. Radmilovic, U. Dahmen, Precipitation and aging in Al-Si-Ge-Cu, *Metall. Mater. Trans. A* **32** (2001) 197. <https://doi.org/10.1007/s11661-998-0335-3>
19. L. Zhang, J. Gao, L. N. W. Damoah, and D. G. Robertson, Removal of iron from aluminum: A review, *Miner. Process. Extr. Metall. Rev.* **33** (2012) 99. <https://doi.org/10.1080/08827508.2010.542211>.
20. A. Canales, J. Talamantes-Silva, D. Gloria, S. Valtierra, and R. Colas, Thermal analysis during solidification of cast Al-Si alloys, *Thermochim. Acta* **510** (2010) 82. <https://doi.org/10.1016/j.tca.2010.06.026>.
21. F. H. Samuel, A. M. Samuel, P. Ouellet, H. W. Doty, Effect of mg and sr additions on the formation of intermetallics in Al- 6 wt pct Si-3.5 Wt pct Cu-(0.45) to (0.8) Wt pct fe 319-type alloys, *Metall. Mater. Trans. A* **29** (1998) 2871. <https://doi.org/10.1007/s11661-998-0194-y>.
22. O. Elsebaie *et al.*, The role of alloying additives and aging treatment on the impact behavior of 319 cast alloy, *Mater. Des.* **32** (2011) 3205. <https://doi.org/10.1016/j.matdes.2011.02.047>.
23. A. M. Samuel, F. H. Samuel, Effect of melt treatment, solidification conditions and porosity level on the tensile properties of 319.2 endchill aluminium castings, *J. Mater. Sci.* **30** (1995) 4825. <https://doi.org/10.1007/BF01154490>.
24. N. S. Tiedje, J. A. Taylor, M. A. Easton, Feeding and distribution of porosity in cast Al-Si alloys as function of alloy composition and modification, *Metall. Mater. Trans. A* **43** (2012) 4846. <https://doi.org/10.1007/s11661-012-1308-0>.
25. N. Roy, A. M. Samuel, and F. H. Samuel, Porosity formation in Al-9 Wt pct Si-3 Wt pct Cu alloy systems: Metallographic observations, *Metall. Mater. Trans. A* **27** (1996) 415. <https://doi.org/10.1007/BF02648419>.
26. J. Campbell, M. Tiryakioglu, Review of effect of P and Sr on modification and porosity development in Al-Si alloys, *Mater. Sci. Technol.* **26** (2010) 262. <https://doi.org/10.1179/174328409X425227>.
27. A. Wiengmoon *et al.*, HRTEM and HAADF-STEM of precipitates at peak ageing of cast A319 aluminium alloy, *Micron* **45** (2013) 32. <https://doi.org/10.1016/j.micron.2012.10.009>.
28. S. Weakley-Bollin *et al.*, Modeling the age-hardening behavior of Al-Si-Cu alloys, *Metall. Mater. Trans. A* **35** (2004) 2407. <https://doi.org/10.1007/s11661-006-0221-9>.
29. D. Mitlin, J. W. Morris, Jr., and V. Radmilovic, Catalyzed precipitation in Al-Cu-Si, *Metall. Mater. Trans. A* **31** (2000) 2697. <https://doi.org/10.1007/BF02830329>.
30. D. O. Ovono, I. Guillot, and D. Massinon, The microstructure and precipitation kinetics of a cast aluminium alloy, *Scr. Mater.* **55** (2006) 259. <https://doi.org/10.1016/j.scriptamat.2006.03.065>.
31. J. Espinoza-Cuadra, P. Gallegos-Acevedo, H. Mancha-Molinar, and A. Picado, Effect of Sr and solidification conditions on characteristics of intermetallic in Al-Si 319 industrial alloys, *Mater. Des.* **31** (2010) 343. <https://doi.org/10.1016/j.matdes.2009.06.017>.
32. S. Shabestari, and M. Malekan, Assessment of the effect of grain refinement on the solidification characteristics of 319 aluminum alloy using thermal analysis, *J. Alloys Compd.* **492** (2010) 134. <https://doi.org/10.1016/j.jallcom.2009.11.122>.
33. J. A. Taylor, Iron-containing intermetallic phases in AlSi based casting alloys, *Proc. Mater. Sci.* **1** (2012) 19. <https://doi.org/10.1016/j.mspro.2012.06.004>.
34. M. Vončina, S. Kores, P. Mrvar, and J. Medved, Effect of ce on solidification and mechanical properties of A360 alloy, *J. Alloys Compd.* **509** (2011) 7349. <https://doi.org/10.1016/j.jallcom.2011.04.059>.